PCCP

Accepted Manuscript

ROYAL SOCIETY OF CHEMISTRY

www.rsc.org/pccp

Journal Name

ARTICLE

Elucidating Low-Frequency Vibrational Dynamics in Calcite and Water with Time-Resolved Third-Harmonic Generation Spectroscopy

Liang Wang,[a,b] Weimin Liu[a,b] and Chong Fang*[a,c]

Low-frequency vibrations are foundational for material properties including thermal conductivity and chemical reactivity. To resolve the intrinsic molecular conformational dynamics in condensed phase, we implement time-resolved third-harmonic generation (TRTHG) spectroscopy to unravel collective skeletal motions in calcite, water, and aqueous salt solution *in situ*. The lifetime of three Raman-active modes in polycrystalline calcite at 155, 282 and 703 cm^{-1} is found to be ca. 1.6 ps, 1.3 ps and 250 fs, respectively. The lifetime difference is due to crystallographic defects and anharmonic effects. By incorporating a home-built wire-guided liquid jet, we apply TRTHG to investigate pure water and $ZnCl_2$ aqueous solution, revealing ultrafast dynamics of water intermolecular stretching and librational bands below 500 cm^{-1} and a characteristic 280 cm^{-1} vibrational mode in the $ZnCl_4(H_2O)_2^{2-}$ complex. TRTHG proves to be a compact and versatile technique that directly uses the 800 nm fundamental laser pulse output to capture ultrafast low-frequency vibrational motion snapshots in condensed-phase materials including the omnipresent water, which provides the important time dimension to spectral characterization of molecular structure-function relationships.

Received 00th March 20xx,
Accepted 00th March 20xx

DOI: 10.1039/x0xx00000x

www.rsc.org/

Introduction

Phonons, together with charge carriers, play an essential role in determining properties of condensed matter including thermal and electrical conductivities. Recent research on thermoelectrics has revived the need to measure acoustic and optical phonons to uncover how those low-frequency lattice motions affect energy transport in solid-state materials.[1,2] Despite technical advances, it remains challenging to track phonon dynamics on molecular timescales,[3] which hinders fundamental understanding and rational design of new functional materials in condensed phase.[4,5] In addition to conventional Raman and infrared spectroscopy, ultrafast optical techniques have been developed to investigate ultrafast phonon and charge carrier dynamics on the timescale of femtosecond (fs) to picosecond (ps), including transient absorption or reflectance measurement,[6,7] second-harmonic generation,[8] sum-frequency generation,[9] and terahertz spectroscopy.[10-12] Theoretical and computational efforts have also aided in modelling phonon and charge dynamics.[13-15] However, crucial information about phonon evolution in solid-state material is still lacking. The extension of phonon studies to liquid (e.g., water) becomes more problematic because low-frequency vibrations are intrinsically difficult to detect in more random and disordered states.[16-18]

In this work, we select calcite as the first molecular paradigm because it is one of the most abundant crystals on earth with extraordinary nonlinear optical properties and extensively studied phonon motions.[13,19,20] To elucidate the ultrafast phonon dynamics, we implement time-resolved third-harmonic generation (TRTHG) spectroscopy which has been recently demonstrated with high sensitivity to phonon motions in solid-state materials such as polycrystalline CaF_2 and amorphous BK7 glass.[21-23] New information on phonon lifetime in calcite is obtained (see below). We hereby extend spectral characterization of low-frequency vibrational motions to pure water and aqueous electrolyte (i.e., 4 M $ZnCl_2$ salt solution) by implementing a home-built flowing liquid sample jet system and comparing to tunable femtosecond stimulated Raman spectroscopy (FSRS) results in the low-frequency region.[24-26] The structural dynamics insights are retrieved that deepen our fundamental understanding of phonon motions in condensed phase, and provide targeted design principles for functional materials with improved thermal and electrical properties.

Results and discussion

[a] *Oregon State University, Department of Chemistry, 263 Linus Pauling Science Center (lab), 153 Gilbert Hall (office), Corvallis, OR 97331, USA. *E-mail: Chong.Fang@oregonstate.edu; Fax: +1 541 737 2062; Tel: +1 541 737 6704*
[b] *These authors contribute equally to this work.*
[c] *Oregon State University, Center for Sustainable Materials Chemistry, 153 Gilbert Hall, Corvallis, OR 97331, USA*

† Electronic Supplementary Information (ESI) available: Additional discussion on lower-frequency phonons in calcite, vibrational quantum beats in TRTHG signal, and the resolving power of TRTHG spectroscopy, comparison between the double and triple-sine-wave numerical fitting results for the TRTHG intensity quantum beats in calcite, comparison between the single and double-sine-wave fitting of the TRTHG intensity quantum beats in pure water, power dependence of the amplitude of vibrational quantum beats observed in TRTHG, additional Figures S1—S3, and references. See DOI: 10.1039/x0xx00000x

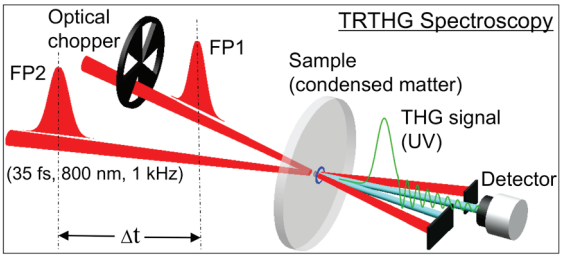

Scheme 1 TRTHG setup utilizes two incident fs-laser pulses and generates a UV signal to detect the vibrational dynamics.

In the optical setup (Scheme 1), because calcite weakly absorbs 800 nm light (~90% transmission, probably due to impurities and defects), some electronic resonance is achieved in the medium via one field interaction with the first pump pulse. The time-dependent polarization from those oscillating electric dipoles created by the first fs-pulse interacts with another time-delayed fs-pulse and scatters THG signals in the phase-matching directions beyond the first pump pulse duration.[22,23] Notably, higher structural order leads to longer-lived signal intensity quantum beats (mainly contributed by vibrational coherences)[27] hence larger detection time window in TRTHG, which corroborate that the initial fs pulse interacts with the medium to generate a transient electronic response that decays on the fs to ps timescale.[23,28,29] We selectively probe the background-free THG signal emitted in the $\bar{k}_1+2\bar{k}_2$ phase-matching direction (see Experimental Section below), confirmed by power dependence measurements as Fig. 1 shows that the THG signal intensity close to time zero delay increases linearly (0.85≈1) with pulse 1 intensity but quadratically (1.84≈2) with pulse 2 intensity. In particular, the medium non-resonant response leads to the dominant THG signal around time zero of the two incident pulses that shows a decay close to the ~35 fs pulse duration, while the electronically resonant response (e.g., evinced by the ~260 fs decay time constant in Fig. 2a) enables us to probe molecular vibrational dynamics beyond the incident pulse duration via the much weaker but still detectable TRTHG signal.

The first incident broadband pulse also generates coherent phonons on the electronic ground state (S_0) via impulsive stimulated Raman scattering (ISRS).[21,30-32] The transient coherent phonons damp on the ps timescale in S_0 while modulating material polarization via cubic nonlinear electric susceptibility $\chi^{(3)}$, which has a time-dependent quantity from the equilibrium value perturbed by an atomic position-dependent term on the ultrafast timescale,

$$\chi^{(3)}(t) = \chi_0^{(3)} + \left(\partial\chi^{(3)}/\partial Q\right)\cdot Q(t) \quad (1)$$

where $\left(\partial\chi^{(3)}/\partial Q\right)$ represents the Raman-type nonlinearity and $Q(t)$ stands for the low-frequency (typically skeletal) vibrations in a molecular system (e.g., lattice motions in a crystal).[33,34] Scheme 2 shows the ISRS process that consists of two field interactions from the first incident laser pulse $\bar{k}_1$ while the initial vibronic configuration in the electronic and vibrational ground state is represented by |g,0>. Once the vibrational coherence is impulsively generated in the medium from time zero upon interaction with the first fs-pump pulse, it will continue to modulate the time-dependent third-order polarizability according to eqn (1) hence the oscillations in TRTHG signal intensity (see ESI† for detailed discussion). This essentially decouples the generation of coherent phonons from time-delayed THG signal generation while the decaying vibrational quantum beats can be retrieved on the basis of eqn (1). Notably, the persistence of coherent phonons in S_0 on the ps timescale before complete damping enables us to track vibrational quantum beating on that timescale and infer the structural dynamics. The shorter timescale for the impulsively generated electronic resonance bolsters the assignment of these transient phonon modes (with fs to ps lifetime in our samples) as coherent wavepackets evolving in S_0.[35]

By tuning time delay between the two incident 800 nm pulses, we obtain clear oscillatory signals superimposed on the THG intensity decay profile from light-matter interactions by the incident fundamental pulses (FPs), which are then Fourier

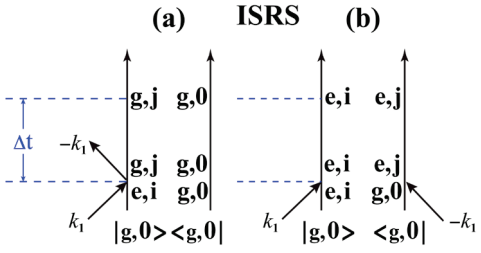

Scheme 2 Feynman diagrams depicting the ISRS process that generates the low-frequency vibrational coherence being detected. (a) Two interactions on the ket side of the density matrix yield the coherent vibrational mode such as an optical phonon wavepacket (e.g., labeled as *i* and *j* for various vibrational level coherences) on the electronic ground state S_0. (b) One interaction on the ket side with one concomitant interaction on the bra side result in coherent vibrational wavepacket motions in the electronic excited state (e.g., S_1). The time delay between the two incident pulses is marked as Δt, during which time the electronic coherence dephasing occurs in the medium hence the THG intensity decrease (see text) while the vibrational coherence generated from ISRS in S_0 decays with typically longer time constants.

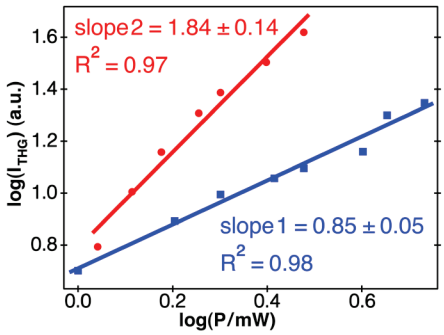

Fig. 1 The observed THG signal strength dependence on the incident pulse intensities. I_{THG} emitted along the phase-matching direction of $\bar{k}_1+2\bar{k}_2$ increases with pulse 1 power to the first order (blue squares, experimental data; blue solid line, fits) while with pulse 2 power to the second order (red dots, experimental data; red solid line, fits). The least-squares fitting R^2 values are noted.

transformed to yield the underlying low-frequency coherent modulation modes in crystal lattice (calcite) and H-bonding network (water and aqueous electrolyte solution, see below).

In the nonlinear response function of condensed-phase samples, both electronic and nuclear responses contribute, though the initial electronic response (typically on the sub-fs timescale) is much faster than the nuclear response (fs to ps timescale). Because calcite absorbs in the 800 nm region (~10% absorption), some electronic coherence is achieved, which may be evinced by the ~260 fs decay time constant with a small weight (Fig. 2a) inferring the free induction decay (FID) of the nascent electronic oscillating dipoles in the medium.[36] To expose atomic motions, we analyze TRTHG signal after ~60 fs by fitting the overall intensity decay to double exponentials (Fig. 2a) and extracting the residual oscillatory component (Fig. 2b). The dominant non-resonant decay time constant is ~38 fs, consistent with the incident pulse duration of ~35 fs. The THG signal continues to drop to a small, almost constant but nonzero background after ~2 ps, which mainly arises from the scattering of THG signal *constantly* generated along the FP1 direction (i.e., $3\vec{k}_1$), which does not exhibit quantum beats in our detection scheme. We confirm this point by blocking FP1 that is being chopped and this signal background diminishes.

Fig. 2c shows the fast Fourier transform (FFT) of intensity oscillations that disappear within ~4 ps, revealing a number of lattice vibrations in calcite. Due to the FP1 bandwidth, three low-frequency modes below 800 cm^{-1} are impulsively excited and they match the frequencies in the standard Raman spectrum but not the relative intensity ratios. This is because the first laser excitation coherently drives Raman transitions (see Fig. S3 for the power dependence data of vibrational quantum beating amplitude in ESI†).[30,31] Upon normalizing the TRTHG-FFT and standard spontaneous Raman spectra to the 282 cm^{-1} peak, the 155 (703) cm^{-1} mode retrieved from FFT is stronger (weaker) than the corresponding Raman mode, respectively, correlating with higher (lower) intensity of incident photons within the pulsed laser bandwidth (Fig. 2c insert). This confirms the impulsive excitation nature of the observed modulation modes (Scheme 2) for TRTHG detection, which enhances the lower-frequency phonon modes that play a typically more important role in governing thermal energy transport properties of condensed-phase functional materials.

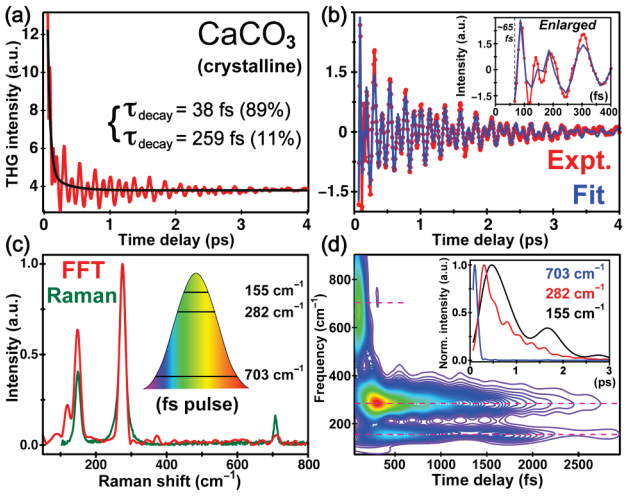

Fig. 2 TRTHG spectroscopy on calcite. (a) The intensity data (red solid trace) show clear time-dependent oscillations within 4 ps. Note that the dominant THG signal around time zero is truncated. The incoherent decay is fitted bi-exponentially (black solid curve) with weighted time constants noted in the insert. (b) The extracted oscillatory component (red circle line) with triple-sine-wave fitting results (blue line). The insert shows the enlarged plot up to 400 fs. (c) The FFT spectrum (red solid trace) is overlaid with the standard Raman spectrum of calcite crystal (green solid trace), normalized to the 282 cm^{-1} peak height. The insert depicts the broadband FP1 pulse that impulsively drives coherent phonon motions. (d) The wavelet transform contour plot of the time-resolved frequency components from the THG intensity quantum beats. The slices through three peak positions (magenta dashed lines) are normalized and plotted against delay time and shown in the insert.

In comparison to standard Raman peaks with Lorentzian lineshape, the FFT spectrum in Fig. 2c shows that all the dominant peaks can be fitted using Gaussian profiles with small error,[24,36,37] indicative of strong inhomogeneous effect from those transiently generated optical phonon modes in the calcite sample. Four classes of crystallographic defects could contribute: (1) point defects like vacancy and interstitial defects, (2) line defects including dislocations, (3) planar defects such as grain boundaries, and (4) bulk defects.[34,38] Another contributing factor arises from the ways the experiments are performed. In spontaneous Raman conducted with a continuous-wave (cw) laser, sharp vibrational modes without phase relations or anharmonic effects are generated. However, in TRTHG spectroscopy, the preceding fs-pulse simultaneously excites all the Raman modes within its broad spectral bandwidth via stimulated Raman processes.[30,32,39] Following fs photoexcitation, these coherent vibrational motions interact with one another during structural evolution that provides various energy dissipation pathways hence the observed Raman peak inhomogeneity.[24]

To dissect the temporal evolution of phonons, we perform Morlet wavelet transform[40] of the THG oscillatory component. The 2D frequency-time intensity contour plot in Fig. 2d without any fitting clearly shows three distinct, transient phonon modes. Furthermore, the phonon intensity shows a mode-dependent rise with the higher-frequency mode displaying the fastest rise and decay, consistent with early-time energy transfer toward lower-frequency phonons via anharmonic coupling (see additional discussion in ESI†).[41] Generally speaking, the observed decay rate difference could be essentially caused by vibrational mode relaxation into the bath modes consisting of many low-frequency modes.[34,42] The density of the bath modes is higher at high energy so that the high-frequency modes have more vibrational energy relaxation pathways and shorter lifetimes. However, in the initial steps to calculate phonon intensity at a certain frequency, the wavelet basis is only partially overlapped with the target signal in the time domain, making it difficult to precisely extract lifetime especially for the short-lived modes with broad linewidth (e.g., 703 cm^{-1}). On the other hand, the higher-frequency modes are typically resolved faster near time zero in wavelet transform (see Fig. 2d) because their vibrational periods are shorter than

those of the lower-frequency modes. To further substantiate the lifetime retrieval from TRTHG data, we build on the FFT analysis and wavelet transform results that confirm the existence of three characteristic optical phonons in crystalline calcite, and numerically fit the coherent quantum beats in Fig. 2b with triple decaying sine waves,

$$S(t) = \sum_{i=1}^{3} A_i e^{-t/\tau_i} \sin(\omega_i t + \varphi_i) \quad (2)$$

where A_i, τ_i, ω_i and φ_i represent each vibrational mode amplitude, lifetime, frequency and phase, respectively. The extracted multiple phonon frequency and lifetime from this least-squares-fitting method can be accurately determined with a standard deviation (s.d.) error of <5%, representing an effective experimental method to dissect vibrational dynamics when a number of low-frequency modes contribute in tandem to the observed quantum beats.

The fitting reveals that the 155, 282 and 703 cm^{-1} modes have the lifetime of ca. 1.6 ps, 1.3 ps and 250 fs, respectively (Fig. S1 in ESI†). Why is the 703 cm^{-1} mode ephemeral? From vibrational normal mode analysis, the 155 cm^{-1} mode corresponds to out-of-phase translation of the carbonate ions parallel to the (111) plane of the rhombohedral cell. The 282 cm^{-1} mode is assigned to librations of the carbonate ions around the two-fold symmetry axes. The 703 cm^{-1} mode is associated with the symmetric deformation of planar CO_3 units.[13,43] The two lower-frequency modes involve translations between Ca^{2+} and CO_3^{2-} with no relative atomic motion within the carbonate ions. However, in the 703 cm^{-1} mode, the four atoms move in the center of mass system of CO_3^{2-} and experience more internal "frictions" to damp the coherent phonon motions, leading to a reduced lifetime. Moreover, the process by which high-frequency strongly interacting phonons decay into low-frequency weakly interacting phonons without breaking energy and momentum conservation is a significant factor shortening the phonon lifetime (see ESI†).[41] Lastly, since a phonon is essentially a travelling mechanical wave in a medium, various phonons respond to defects in different ways during propagation.[38] Low-frequency optical phonons with long wavelengths have high tolerance for the size of defects due to their stronger diffraction ability. In contrast, high-frequency modes are more vulnerable to local defects because they are more likely to be scattered and damped.

One major advantage of TRTHG is the elucidation of transient phonon dynamics. Typically, the lifetime of a phonon mode can be estimated from its spectral width (full-width-at-half-maximum or fwhm, $\Delta\omega$) using energy-time uncertainty,

$$\Delta\omega \cdot \tau = 1/2\pi c \quad (3)$$

with the value of about 5.3 ps·cm^{-1} for the (vibrational population relaxation) lifetime-dominated spectral line broadening mechanism.[32,41,44,45] Besides instrumental factors, this method neglects other factors such as crystallographic defects and anharmonic effects that influence peak width, which can be accounted for by a scaling factor. Notably, TRTHG enables detection of coherent phonon dynamics starting from time zero of photoexcitation, and the mode-dependent lifetime measurement. The observed fwhm and lifetime of three dominant phonon modes at 155, 282, 703 cm^{-1} are ca. 19, 20, 25 cm^{-1} and 1.6 ps, 1.3 ps, 250 fs, respectively (see above). The product of fwhm and lifetime deviates from 1 (see eqn (3)), confirming that other broadening factors contribute to the peak width.[46] Moreover, with an additional 800 nm pulse, 2D TRTHG has been recently demonstrated in our lab that may provide a compact alternative setup for 2D UV spectroscopy,[36,47] and will be reported in a future publication.

The success of TRTHG to reveal solid-state phonon dynamics motivates us to explore more potential applications of this technique. Molecular vibrations in liquids are crucial in chemical reactions.[48] Particularly, low-frequency skeletal motions play a key role in excited-state proton transfer.[49-52] However, liquids are intrinsically disordered and molecules in liquids can move on ultrafast timescales. Low-frequency vibrations, especially those related to intermolecular forces in liquids, are thus challenging to capture. Can we study the low-frequency vibrational dynamics in solution by incorporating a home-built flowing liquid sample jet to the TRTHG setup? The key is to achieve the spectral and temporal resolutions needed to elucidate the conformational motions of solvent and solute molecules. We start with pure water, the omnipresent solvent and also the "matrix of life". The TRTHG data (Fig. 3a) clearly display intensity quantum beats within 1 ps, which is shorter than the calcite detection time window (Fig. 2a). The double-sine-wave fitting in Fig. 3b after subtracting the incoherent THG signal exponential decay component reveals a dominant modulation mode at ~385 cm^{-1} with a lifetime of 66±8 fs (see reproducibility in Fig. S2 in ESI†). We assign this Raman mode

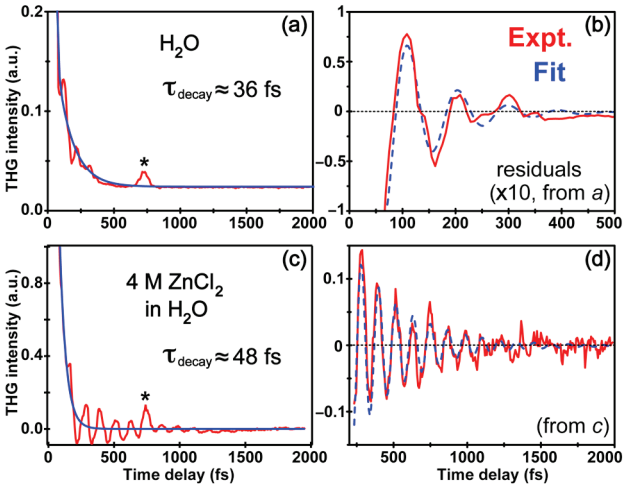

Fig. 3 TRTHG spectra of water and 4 M $ZnCl_2$ aqueous solution. (a) The raw data of H_2O (red) and the single-exponential fit (blue) that is mainly related to the autocorrelation profile of the incident pulses. (b) The sub-ps coherent oscillatory component from (a) in red solid trace is numerically fitted by a sum of decaying sine waves in blue dashed trace. (c) The raw data of 4 M $ZnCl_2$ aqueous solution (red) and the single-exponential fit (blue). Similar to (a), the asterisk denotes an anomaly at ~730 fs that may arise from a front-back-surface double reflection of the flowing liquid film with a thickness of ~100 μm. (d) The coherent oscillatory component from (c) in red solid trace is numerically fitted by a decaying sine wave in blue dashed trace.

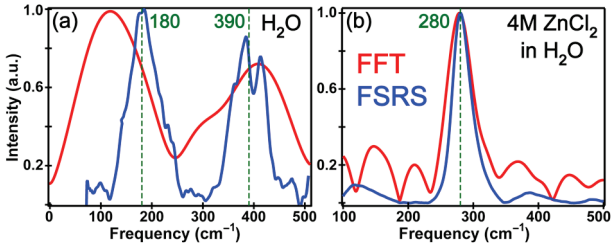

Fig. 4 Comparison between the FFT spectrum (red) of the TRTHG intensity quantum beats shown in Fig. 3 and the ground-state femtosecond stimulated Raman spectroscopy (FSRS) spectrum (blue, with 580 nm Raman pump) below 500 cm^{-1} of pure water (a) and 4 M $ZnCl_2$ aqueous solution (b), respectively.

to an intermolecular vibration within the water librational band[53-55] that significantly modulates the cubic nonlinear electric susceptibility $\chi^{(3)}$ of the medium (see eqn (1)).[34,56] The broad peak at ~160 cm^{-1} with a lifetime of 130±15 fs likely consists of the H-bond O–H···O stretching mode at ~180 cm^{-1} in water,[57] which is a translational motion that receives much less energy than rotational degrees of freedom on the sub-100 fs timescale[58] and exerts less influence on the nascent THG signal (see relative weight of the fitted components following Fig. S2 in ESI†). These results based on our new experimental data demonstrate the resolving power of TRTHG in capturing equilibrium skeletal motions of liquid samples such as water. In comparison to terahertz (THz) spectroscopy that is a powerful technique studying low-frequency modes in molecular systems,[11,12,59,60] TRTHG has a simpler optical setup (e.g., no nonlinear crystal for THz pulse generation), higher time resolution (e.g., exposing multiple mode lifetimes on the fs timescale), and specificity in observing microscopic molecular dynamics corresponding to the higher-frequency (typically >100 cm^{-1}) processes in dielectric spectrum in the THz domain.[61] To further confirm the observed low-frequency Raman-active modes below 500 cm^{-1}, we use our newly developed tunable FSRS setup in the same laboratory to measure the ground-state Raman modes of pure water (see Experimental Section). The comparison between the FFT spectrum of TRTHG oscillatory data and the FSRS spectrum[24,62] in Fig. 4a clearly corroborates the assignment of the two broad peaks to the reported H-bond stretching and librational modes in water.[17,57,58]

To overcome signal-to-noise issues and substantiate the TRTHG capability to reveal solution "phonon" modes, we continue to study low-frequency vibrations with greater polarizability and longer lifetime. Transition metal complexes typically have large electronic polarizability due to oppositely charged metal center and ligands. Fig. 3c shows the TRTHG data on 4 M $ZnCl_2$ aqueous solution with pronounced quantum beats (Fig. 3d) which represent a new case study for low-frequency vibrational motions of electrolytes dissolved in water. The underlying vibrational mode from fitting (see eqn (2) but with a single decaying sine wave) is at ~285 cm^{-1} (~280 cm^{-1} in the FFT spectrum, Fig. 4b) with a lifetime of 370±25 fs. This mode is a characteristic symmetric stretching band ($\nu_1 a_{1g}$, D_{4h} point group) of $ZnCl_4(H_2O)_2^{2-}$ complex in 4 M $ZnCl_2$ aqueous solution, supported by both experimental and theoretical reports.[63-65] This result also nicely matches our ground-state FSRS spectrum that shows a dominant 280 cm^{-1} peak (Fig. 4b). The increase of observed vibrational mode lifetime in comparison to pure water (~100 fs) as well as narrower linewidth in Fig. 4b versus 4a (see eqn (3)) suggests that more structural order is established in the $ZnCl_2$ aqueous solution, particularly in the first solvation shell of the dominant $ZnCl_4(H_2O)_2^{2-}$ complex (i.e., the Zn^{2+} ion coordinates four Cl^- ions in a single plane and two H_2O molecules above and below the plane, respectively). We expect to use TRTHG spectroscopy to study other aqueous electrolytes and benchmark the structural dynamics basis for coordination chemistry in a H-bonding network on the intrinsic molecular timescale.

Experimental

Briefly, an fs Ti:sapphire laser regenerative amplifier (Legend Elite-USP, Coherent) seeded by an oscillator (Mantis, Coherent, Inc.) provides fundamental pulses (FPs) with 35 fs pulse duration, 800 nm center wavelength at 1 kHz repetition rate. A portion of the *p*-polarized FP is divided by a beamsplitter (50R/50T) into two arms with ~50 μJ/pulse energy each, attenuated by an iris and a variable neutral density filter. Both arms (FP1 and FP2 in Scheme 1) are set to 6 μJ pulse energy. The two noncollinear FPs are spatially overlapped in a Gaussian spot on the 1-mm-thick calcite crystal plate using an *f*=10 cm Ag-coated concave mirror, with beam diameters of ~0.2 mm at the foci and ~6° crossing angle. The calcite crystal is rotated to achieve maximal UV signal generation at the THG Type-I phase-matching angle.[66] In reality, the angle tuning of crystal orientation is performed to minimize Δk, which reaches zero for perfect phase matching in the collinear setup (wherein the wavevector scalar $k(\omega) = n(\omega)\omega/c$, $n(\omega)$ is the frequency-dependent refractive index, ω is angular frequency, and c is vacuum light velocity). Notably, the THG signal wavelength we detect in between the two incident laser beams (Scheme 1) differs from that emitted collinearly with the incident beams (i.e., $3\vec{k}_1$ or $3\vec{k}_2$) in accordance with the actual (geometrical) phase-matching conditions.[22] Moreover, because bulk water is not birefringent material like calcite crystal, the phase mismatch is larger and the observed THG signal strength is much weaker in thin water film than that in crystalline calcite.

A high-resolution motorized delay stage (07EAS504, CVI Melles Griot) controls the time delay between the two incident pulses. FP1 is chopped at 500 Hz by a phase-locked optical chopper (3501, Newport). To increase the coherent phonon generation efficiency and minimize the FP-THG scattering, we monitor the THG signal after a UV-bandpass filter (FGUV11, Thorlabs) on the unchopped FP2 beam side (see Scheme 1) and Si photodiode detector.[23] The phase-matching condition of the resultant THG signal is $\vec{k}_1 + 2\vec{k}_2$, and its intensity is detected with a step size of ~6.67 fs through a lock-in amplifier synchronized to the phase-stable optical chopper. All the experimental data are collected at ambient pressure and room temperature of 22 °C.

In the liquid sample jet, liquid is pumped to upper reservoir by a peristaltic pump from the bottom reservoir. The upper reservoir is open to air and has a bypass to maintain constant liquid pressure. Driven by gravity, liquid sample flows from the upper reservoir and forms a thin film between two parallel Ti wires when it exits the jet vertically. After the sample catcher, liquid sample is recycled from the bottom reservoir and pumped upward. For femtosecond Raman measurements, a newly developed wavelength tunable FSRS setup[62] is used to generate the Raman pump pulse at 580 nm, ~2 ps, 8 mW, and a much weaker fs broadband probe pulse to the red side of the Raman pump. The much higher pulsed laser peak density, the stimulated nature of Raman scattering, and the efficient data averaging at ~2 ms/spectrum (i.e., CCD camera synchronized with the 1 kHz laser repetition rate and the optical chopper operating at 500 Hz)[25] makes the signal-to-noise ratio much higher than the cw Raman detection scheme. Both pure water (Millipore) and 4 M $ZnCl_2$ in aqueous solution are measured in a 1-mm-pathlength quartz flow cell (48-Q-1, Starna) on the same day, and 180,000 Raman spectra are collected and averaged for each sample.[24] At least three independent measurements are performed on each sample to ensure reproducibility (see Fig. S2 for example). Notably, the observed spectral oscillations all decay away within our detection time window (see Figs. 2b, 3b, and 3d) so the Fourier transform exposes the underlying modulation modes without significant apodization requirement or peak broadening, which enables us to retrieve the vibrational mode-specific lifetime information and correlate with molecular structural motions.

Conclusions

In summary, we have investigated coherent low-frequency vibrational dynamics in condensed phase using the newly developed background-free TRTHG spectroscopy. The surface specificity of THG has been demonstrated and could be beneficial to probe interfacial boundaries.[21-23,67] For the first time, we reveal lifetimes of three optical phonons in calcite crystal lattice and attribute the structural dynamics origin to crystallographic defects, system-bath coupling and anharmonic effects in the medium. The lower-frequency modes are enhanced due to the impulsive excitation of coherent phonons by the fs near-IR laser pump pulse which may prove instrumental to study thermal transport. Upon integration with a home-built liquid sample jet, TRTHG is capable of revealing low-frequency vibrational motions in liquid phase from pure water to aqueous electrolyte solution such as $ZnCl_2$. We obtain the water librational band at ~385 cm^{-1} with a lifetime of ~70 fs, and a lengthened lifetime (~370 fs) of the 285 cm^{-1} characteristic band associated with the $ZnCl_4(H_2O)_2^{2-}$ complex. The Raman-active mode frequency retrieved from FFT analysis of TRTHG signal oscillations is corroborated by tunable FSRS results in the low-frequency region. These synergistic experimental data showcase the unique power and high sensitivity of TRTHG spectroscopy to spectrally and temporally characterize low-frequency vibrational motions in condensed phase, which open new avenues with simplicity and versatility to obtain structural dynamics insights and rational design principles for improved functional materials in a wide range of energy and biology-related fields.

Acknowledgements

This research was supported by the Oregon State University Faculty Start-up Research Grant and General Research Fund Award to C.F. We thank Liangdong Zhu (research fellowship from the NSF Center for Sustainable Materials Chemistry, grant number CHE-1102637) for help with experiments and Breland Oscar for helpful discussions. We also acknowledge the recent NSF CAREER Award (CHE-1455353) to C.F.

Notes and references

1 D. G. Cahill, P. V. Braun, G. Chen, D. R. Clarke, S. Fan, K. E. Goodson, P. Keblinski, W. P. King, G. D. Mahan, A. Majumdar, et al., *Appl. Phys. Rev.*, 2014, **1**, 011305.
2 M. Gilbert and B. Albinsson, *Chem. Soc. Rev.*, 2015, **44**, 845-862.
3 A. H. Zewail, *Femtochemistry: Ultrafast Dynamics of the Chemical Bond*, World Scientific, Singapore, 1994.
4 W. A. Kutt, W. Albrecht and H. Kurz, *IEEE J. Quantum Electron.*, 1992, **28**, 2434-2444.
5 K. Ramasesha, L. De Marco, A. Mandal and A. Tokmakoff, *Nat. Chem.*, 2013, **5**, 935-940.
6 J. Qi, X. Chen, W. Yu, P. Cadden-Zimansky, D. Smirnov, N. H. Tolk, I. Miotkowski, H. Cao, Y. P. Chen, Y. Wu, et al., *Appl. Phys. Lett.*, 2010, **97**, 182102.
7 G. C. Cho, W. Kutt and H. Kurz, *Phys. Rev. Lett.*, 1990, **65**, 764-766.
8 Y. M. Chang, L. Xu and H. W. K. Tom, *Phys. Rev. Lett.*, 1997, **78**, 4649-4652.
9 Y. R. Shen, *J. Opt. Soc. Am. B*, 2011, **28**, A56-A66.
10 G. C. Cho, P. Y. Han, X.-C. Zhang and H. J. Bakker, *Opt. Lett.*, 2000, **25**, 1609-1611.
11 U. Heugen, G. Schwaab, E. Bründermann, M. Heyden, X. Yu, D. M. Leitner and M. Havenith, *Proc. Nat. Acad. Sci. U.S.A.*, 2006, **103**, 12301-12306.
12 J. Savolainen, S. Ahmed and P. Hamm, *Proc. Nat. Acad. Sci. U.S.A.*, 2013, **110**, 20402-20407.
13 M. Prencipe, F. Pascale, C. M. Zicovich-Wilson, V. R. Saunders, R. Orlando and R. Dovesi, *Phys. Chem. Minerals*, 2004, **31**, 559-564.
14 J. A. Thomas, J. E. Turney, R. M. Iutzi, C. H. Amon and A. J. H. McGaughey, *Phys. Rev. B*, 2010, **81**, 081411(R).
15 S. Petros, *J. Phys.: Condens. Matter*, 2011, **23**, 445401.
16 J. T. Hynes, *Nature*, 1999, **397**, 565-567.
17 J. L. Skinner, *Science*, 2010, **328**, 985-986.
18 M. Ceriotti, J. Cuny, M. Parrinello and D. E. Manolopoulos, *Proc. Nat. Acad. Sci. U.S.A.*, 2013, **110**, 15591-15596.
19 E. R. Cowley and A. K. Pant, *Phys. Rev. B*, 1973, **8**, 4795-4800.
20 A. Penzkofer, F. Ossig and P. Qiu, *Appl. Phys. B*, 1988, **47**, 71-81.
21 D. Kupka, J. W. Wilson, O. Masihzadeh and R. A. Bartels, *Chem. Phys. Lett.*, 2010, **490**, 97-101.
22 W. Liu, L. Wang, F. Han and C. Fang, *Opt. Lett.*, 2013, **38**, 3304-3307.
23 W. Liu, L. Wang, F. Han and C. Fang, *Appl. Phys. Lett.*, 2013, **103**, 201116.

24 W. Liu, F. Han, C. Smith and C. Fang, *J. Phys. Chem. B*, 2012, **116**, 10535-10550.
25 F. Han, W. Liu and C. Fang, *Chem. Phys.*, 2013, **422**, 204-219.
26 W. Wang, W. Liu, I.-Y. Chang, L. A. Wills, L. N. Zakharov, S. W. Boettcher, P. H.-Y. Cheong, C. Fang and D. A. Keszler, *Proc. Natl. Acad. Sci. U.S.A.*, 2013, **110**, 18397-18401.
27 D. B. Turner, K. E. Wilk, P. M. G. Curmi and G. D. Scholes, *J. Phys. Chem. Lett.*, 2011, **2**, 1904-1911.
28 T. Utikal, M. I. Stockman, A. P. Heberle, M. Lippitz and H. Giessen, *Phys. Rev. Lett.*, 2010, **104**, 113903.
29 A. D. Jameson, J. L. Tomaino, Y.-S. Lee, G. Khitrova, H. M. Gibbs, C. N. Böttge, A. C. Klettke, M. Kira and S. W. Koch, *Optica*, 2014, **1**, 276-280.
30 S. De Silvestri, J. G. Fujimoto, E. P. Ippen, E. B. Gamble, Jr., L. R. Williams and K. A. Nelson, *Chem. Phys. Lett.*, 1985, **116**, 146-152.
31 A. Nazarkin and G. Korn, *Phys. Rev. A*, 1998, **58**, R61-R64.
32 P. Kukura, D. W. McCamant and R. A. Mathies, *Annu. Rev. Phys. Chem.*, 2007, **58**, 461-488.
33 R. Merlin, *Solid State Commun.*, 1997, **102**, 207-220.
34 M. Born and K. Huang, *Dynamical Theory of Crystal Lattices*, Oxford University Press, USA, New York, NY, 1998.
35 K. L. Litvinenko and S. R. Meech, *Phys. Chem. Chem. Phys.*, 2004, **6**, 2012-2014.
36 R. M. Hochstrasser, *Proc. Natl. Acad. Sci. U.S.A.*, 2007, **104**, 14190-14196.
37 R. R. Frontiera, C. Fang, J. Dasgupta and R. A. Mathies, *Phys. Chem. Chem. Phys.*, 2012, **14**, 405-414.
38 P. G. Klemens, *Proc. Phys. Soc. A*, 1955, **68**, 1113-1128.
39 A. B. Myers and R. A. Mathies, in *Biological Applications of Raman Spectroscopy*, ed. T. G. Spiro, John Wiley & Sons, Inc., New York, 1987, vol. 2, pp. 1-58.
40 C. Chatfield, *The Analysis of Time Series: An Introduction*, 6th Ed., Chapman & Hall/CRC, Boca Raton, FL, 2004.
41 S. Anand, P. Verma, K. P. Jain and S. C. Abbi, *Phys. B: Condens. Matter*, 1996, **226**, 331-337.
42 H. Ibach and H. Lüth, *Solid-State Physics: An Introduction to Principles of Materials Science*, Springer-Verlag, Berlin Heidelberg, 2009.
43 S. Gunasekaran, G. Anbalagan and S. Pandi, *J. Raman Spectrosc.*, 2006, **37**, 892-899.
44 N. Domènech-Amador, R. Cuscó, L. Artús, T. Stoica and R. Calarco, *Nanotechnology*, 2012, **23**, 085702.
45 P. Pobedinskas, B. Ruttens, J. D'Haen and K. Haenen, *Appl. Phys. Lett.*, 2012, **100**, 191906.
46 C. Fang, J. D. Bauman, K. Das, A. Remorino, E. Arnold and R. M. Hochstrasser, *Proc. Natl. Acad. Sci. U.S.A.*, 2008, **105**, 1472-1477.
47 B. A. West and A. M. Moran, *J. Phys. Chem. Lett.*, 2012, **3**, 2575-2581.
48 E. T. J. Nibbering, H. Fidder and E. Pines, *Annu. Rev. Phys. Chem.*, 2005, **56**, 337-367.
49 C. Fang, R. R. Frontiera, R. Tran and R. A. Mathies, *Nature*, 2009, **462**, 200-204.
50 B. G. Oscar, W. Liu, Y. Zhao, L. Tang, Y. Wang, R. E. Campbell and C. Fang, *Proc. Natl. Acad. Sci. U.S.A.*, 2014, **111**, 10191-10196.
51 R. Simkovitch, S. Shomer, R. Gepshtein and D. Huppert, *J. Phys. Chem. B*, 2015, **119**, 2253-2262.
52 L. Tang, W. Liu, Y. Wang, Y. Zhao, B. G. Oscar, R. E. Campbell and C. Fang, *Chem. Eur. J.*, 2015, **21**, 6481-6490.
53 D. M. Carey and G. M. Korenowski, *J. Chem. Phys.*, 1998, **108**, 2669-2675.
54 C. J. Fecko, J. D. Eaves, J. J. Loparo, A. Tokmakoff and P. L. Geissler, *Science*, 2003, **301**, 1698-1702.
55 V. A. Babenko and A. A. Sychev, *Quantum Electron.*, 2012, **42**, 839-842.
56 J. L. McHale, *Molecular Spectroscopy*, Prentice-Hall, Upper Saddle River, NJ, 1999.
57 I. A. Heisler and S. R. Meech, *Science*, 2010, **327**, 857-860.
58 J. Petersen, K. B. Møller, R. Rey and J. T. Hynes, *J. Phys. Chem. B*, 2013, **117**, 4541-4552.
59 M. Heyden, J. Sun, S. Funkner, G. Mathias, H. Forbert, M. Havenith and D. Marx, *Proc. Nat. Acad. Sci. U.S.A.*, 2010, **107**, 12068-12073.
60 L. M. Lepodise, J. Horvat and R. A. Lewis, *Phys. Chem. Chem. Phys.*, 2013, **15**, 20252-20261.
61 T. Fukasawa, T. Sato, J. Watanabe, Y. Hama, W. Kunz and R. Buchner, *Phys. Rev. Lett.*, 2005, **95**, 197802.
62 L. Zhu, W. Liu and C. Fang, *Appl. Phys. Lett.*, 2014, **105**, 041106.
63 D. E. Irish, B. McCarroll and T. F. Young, *J. Chem. Phys.*, 1963, **39**, 3436-3444.
64 W. W. Rudolph and C. C. Pye, *Phys. Chem. Chem. Phys.*, 1999, **1**, 4583-4593.
65 C. C. Pye, C. R. Corbeil and W. W. Rudolph, *Phys. Chem. Chem. Phys.*, 2006, **8**, 5428-5436.
66 A. Penzkofer, P. Qiu and F. Ossig, in *Nonlinear Optics of Organics and Semiconductors*, ed. T. Kobayashi, Springer-Verlag, Berlin, Heidelberg, 1989, vol. 36.
67 L. Zhu, W. Liu and C. Fang, *Appl. Phys. Lett.*, 2013, **103**, 061110.